Journal of Thermal Analysis and Calorimetry (2023) 148:12877–12890
https://doi.org/10.1007/s10973-023-12541-2

Study of the acoustic response of a swirl/bluff-body stabilized natural gas flame: experimental aspects and theoretical rationale

M. Behzadi[1] · **E. Movahednejad**[1] · **F. Ommi**[1]

Received: 8 January 2023 / Accepted: 27 August 2023 / Published online: 13 October 2023

Abstract

The thermo-acoustic stability of a combustor may be assessed in its design phase via solving an expression for the interior acoustic field with flame characteristics treated as an input. This input must include the flame response to axial upstream disturbances. Practical details of a response evaluation are expressed for the case of a premixed natural gas burner whose flame is stabilized by means of the combination of swirl and bluff-body. An equation for instability analysis in a gas turbine was derived incorporating a practically-measurable and applicable form of flame response. Velocity disturbances were monitored using a hot-film anemometer and chemiluminescence of heat-release fluctuations using a photomultiplier. The photomultiplier gain sensitivity to the angle of incidence of rays was first determined and taken into account. A method based on coincidence of time series was used to evaluate phase difference between two signals. It was found that the geometry of the settling chamber along with the location of the speakers causes the excitability of the acoustic field experience a sharp peak at 300 Hz which relates to the first natural mode of the chamber. The magnitude of the flame describing function assumes values from nearly zero up to 2.7 depending on frequency and excitation level while the phase depends on frequency only. For the case of the excitations that cause noticeable responses, the ratio of the acoustic wavelengths to the flame length is higher than 30, which shows that a global response for the whole flame instead of a field function may be assumed.

Keywords Thermo-acoustic instability · Premixed swirl burner · Bluff-body stabilization · Photomultiplier · Phase difference

List of symbols

- c Sound speed, m s^{-1}
- f Frequency, Hz
- G Describing function magnitude
- p Pressure, Pa
- q Heat-release-rate, W m^{-3}
- Q Total heat-release-rate, W
- t Time, s
- u Velocity, m s^{-1}
- V Volume, m^3
- x Position, m
- γ Isentropic constant
- ρ Density, kg m^{-3}
- Φ Describing function phase, rad
- ω Angular frequency, rad s^{-1}

Subscripts

- 1 Velocity measurement location
- a Axial
- f Flame
- tot Flame total

✉ M. Behzadi
milad.behzadi@modares.ac.ir

1 Department of Aerospace, Faculty of Mechanical Engineering, Tarbiat Modares University, Tehran, Iran

Introduction

The desirable technology for gas turbine combustors in the last two decades have been lean premixed combustion in order to reduce pollutant emissions especially nitrogen oxide [1, 2]. A combustor must fulfill various requirements including stability over the whole operating range. Compared to diffusion flames, lean premixed flames are more prone to thermo-acoustic instability, which is the result of destructive coupling of heat-release with the acoustic field [3]. The stability of a combustor must be considered in the design process and thus the necessary information for this analysis need to be obtained.

Conventional instability analysis methods can be categorized into two classes. One is based on computational fluid dynamics which must be capable of handling unsteady, compressible, reactive flows [4–6] and is not presented here. The other is based on solving the acoustic filed with flame characteristics treated as an input source term. The equation describing the acoustic filed of a system containing a heat source is Helmholtz equation [7]:

$$\frac{1}{\bar{c}^2}\frac{\partial^2 p}{\partial t^2} - \nabla^2 p = \frac{\gamma - 1}{\bar{c}^2}\frac{\partial q}{\partial t} \tag{1}$$

where c is sonic velocity, q and p are fluctuating heat release rate and pressure, respectively, and γ is isentropic exponent. Fluctuating variables are written without any additional sign for convenience while mean parameters have a bar above. The term on the right hand side of the equation pertains to the flame and is an input to the equation which describes the dependency of heat-release fluctuations on one of the flow parameters. In gas turbines, the flame may respond to both velocity and equivalence ratio fluctuations [8].

This equation may be solved, for simplified geometries, analytically [7] or through the network method [9, 10]. The solution result includes the frequency and the growth rate of the fluctuations. The growth rate may then be compared to the damping rate of the system to determine stability of the system. For complex geometries, the equation may be solved using finite element method. The acoustic field remains linear even when the system reaches a limit cycle level. This is the flame response that is responsible for the nonlinear behavior of the system [10]. Consequently, the flame response need to be defined not only as a function of frequency but also as a function of fluctuation amplitude [11]. This response may be determined experimentally and may also be found using CFD analysis of the flame [12, 13].

The applicability of flame response in analysis has been previously established. If the flame dimensions are negligible compared to the acoustic wavelength, a total response for the whole flame may be defined [10]. This assertion is usually valid especially when tangential acoustic mode in an annular combustor is engaged in instability. Flame heat-release-rate has been found to be mainly influenced by upstream axial acoustic and flow vortical disturbances and not by lateral transverse disturbances [14, 15]. Vortical disturbances themselves are produced by acoustic excitation [16]. The heat-release behavior of a swirl flame in an annular combustor has been shown to be the same as its behavior when excited with axial acoustic disturbances [17].

There are two common methods for measuring flame response, both including artificial excitation of the flame. One method is to document fluctuations of heat-release and inlet velocity of the burner. The other is based on observation of the flame response effect on the acoustic wave [18–20] and may be used for partially or fully premixed flames but not for reaction zone detection. The first method is of current interest.

The techniques proved viable for measurement of heat-release fluctuations are optical methods based on chemiluminescnece [21–23]. Heat-release fluctuation measurement via ion sensing has been used in internal combustion engines [24] and ion current has been shown to be proportional to heat-release in premixed turbulent flames [25] but this method is not yet fully developed and reliable. The candidate radicals for chemiluminescence are OH*, CH*, and C2* [21]. OH* emissions in the UV range and CH* emissions in visible spectrum are more intense in lean to stoichiometry flames and their intensities have proved to be linearly proportional to heat-release-rate [26, 27]. Chemiluminescence may also be used to exactly distinguish the reaction zone [28–30] since the reaction zone and the visible flame does not necessarily coincide. Because of the linear proportionality to heat-release, this phenomena is suitable for fully premixed flames, even though it has been utilized for partially premixed flames too [31]. It is worth noting that in LASER-induced fluorescence, the ions (usually OH, CH, CH2O, and even two ions at the same time [32]) are artificially excited by means of LASER and may be used to detect reaction zone [33, 34] but not to measure heat-release fluctuations. Inlet velocity fluctuations may be measured via LASER Doppler velocimetry, the microphone method [35, 36], or simply by hotwire anemometry.

The premixed flame response to acoustic excitation have been widely studied. First, simple flames and the effect of fluctuating velocity field on flame surface wrinkles were examined [37]. The excitation level was increased to observe nonlinear behavior [23]. Similarity of responses has been studied [38] and a model for the response was presented based on the model for V flame response [39]. However, this model was limited to flames of single-annulus axial swirl burners and failed to predict behavior of flames of different burner geometries [40]. Comparison of the response or describing functions of flames shows that this function is not the same for different burner types, geometries, and also operating conditions, e.g., [41, 42].

The response to acoustic excitation of flame in a new laboratory burner has been examined in the current work. The premixed flame of this burner is stabilized with a combination of swirl and bluff-body for which dynamic behavior is inadequately addressed, especially when swirl is obtained via a radial swirler. It has been recently found that the presence of central body affects flame response for certain frequencies [43, 44]. Further, experimental details of response evaluation have been established. Although flame dynamics have long been studied, practical details have not been presented. Thus, the innovations are in brief (1) presenting the flame response of a new burner that is stabilized by combination of swirl and bluff-body and study of dependency of response on excitation level; and (2) state the considerations of experimental investigation of response in a usable way for others. Theory and governing equations for instability analysis, experimental setup and the numerical method details, results and discussions have been described in succession.

Instability analysis equations and theory

Understanding the details and provisions of obtaining a flame describing function becomes possible when the theory behind its definition and use is clear. It was discussed that a practical method for instability analysis is solving the Helmholtz equation which includes terms related to acoustic field and the flame describing function. Combustion instability in a three-dimensional domain may be analyzed using Eq. (1) but it should be derived to a form suitable for gas turbines and also containing a form of flame response that may be practically obtained. This derivation detail and interpretation of variables could not be found elsewhere. Heat-release fluctuation q is gathered from the whole flame volume V_f and its distribution over the flame is not usually important. This overall value per unit volume is defined as

$$q_{\mathrm{tot}}(t) = \frac{\int_{V_{\mathrm{f}}} q(x,t)\mathrm{d}v}{V_{\mathrm{f}}} = \frac{Q}{V_{\mathrm{f}}} \tag{2}$$

where Q is total heat-release fluctuation. Time derivative of heat-release fluctuation on the right hand side of Eq. (1) may now be written as

$$\frac{\partial q(x,t)}{\partial t} = \frac{\mathrm{d}q_{\mathrm{tot}}(t)}{\mathrm{d}t} = \frac{1}{V_{\mathrm{f}}}\frac{\mathrm{d}Q(t)}{\mathrm{d}t} \tag{3}$$

The heat-release fluctuations are measured using a photomultiplier in the experiments which gives an electrical voltage proportional to the instantaneous heat power. Thus, the absolute value of heat-release fluctuation is neither known nor necessary. Instead, it is easier to count on the ratio of heat-release fluctuation to its mean value $\overline{Q}$. This is well compatible with the definition of flame response:

$$Ge^{\mathrm{i}\phi} = \frac{Q(t)\big/\overline{Q}}{u_{\mathrm{a}}(x_1,t)\big/\overline{u}_{\mathrm{a}}(x_1)}. \tag{4}$$

a and *1* in this equation indicate that axial velocity u_{a} at a specific upstream point x_1 is to be measured which is practical. Remember that as stated in the introduction the response to axial velocity perturbation must be measured. Substitution of equation in 3 gives

$$\frac{\partial q(x,t)}{\partial t} = \frac{\overline{Q}\,G\,e^{i\phi}}{V_{\mathrm{f}}\overline{u}_{\mathrm{a}}\left(x_1\right)}\frac{\partial u_{\mathrm{a}}\left(x_1,t\right)}{\partial t}. \tag{5}$$

With the help of momentum equation, velocity may be related to pressure so that there is one dependent variable left

$$\frac{\partial u_{\mathrm{a}}\left(x_1,t\right)}{\partial t} = -\frac{1}{\overline{\rho}_1}\nabla_{\mathrm{a}}p\left(x_1,t\right) \tag{6}$$

where ∇_{a} means axial gradient. Assuming a special mode shape $\hat{p}(x)$ and temporal periodicity $e^{\mathrm{i}\omega t}$ for pressure, Eq. (5) now becomes

$$\frac{\partial q(x,t)}{\partial t} = -\frac{\overline{Q}\,G\,e^{\mathrm{i}\phi}}{\overline{\rho}_1 V_{\mathrm{f}}\overline{u}_{\mathrm{a}}\left(x_1\right)}\nabla_{\mathrm{a}}\hat{p}\left(x_1\right)\,e^{\mathrm{i}\omega t} \tag{7}$$

This is an appropriate form for the heat-release fluctuation term in Eq. (1) which gives an applicable equation for analysis of instability due to heat-release and velocity coupling.

$$\frac{\omega^2}{\overline{c}^2}\hat{p}(x) + \nabla^2\hat{p}(x) = \frac{\gamma-1}{\overline{c}^2}\frac{\overline{Q}\,G\,e^{\mathrm{i}\phi}}{\overline{\rho}V_{\mathrm{f}}\overline{u}_{\mathrm{a}}\left(x_1\right)}\nabla_{\mathrm{a}}\hat{p}\left(x_1\right) \tag{8}$$

This form of equation may be solved with a finite element commercial software or code. The domain comprises of three zones: the fresh mixture, the flame volume, and the burned hot gases. The homogenous form of this equation holds in the first and the last zones while the source term in the right hand side need to be considered in the flame zone. Solving this equation is an eigenvalue problem that yields the complex frequency and pressure mode shape. All the inputs are simple gas and flame properties except the flame response which may be obtained experimentally. For this purpose, normalized heat-release fluctuations of the whole flame and upstream velocity fluctuation need to be measured.

Experimental setup and numerical method

The burner under examination is a newly built university burner for combustion research for which operating envelope has been recently studied [45]. A plenum was added to facilitate acoustic excitation. Heat-release and velocity fluctuations are measured separately via chemiluminescence and hot-wire anemometry, respectively. Chemiluminescence measurement is a done using a photomultiplier (PM). The capability of this instrument in recording light from different incident angles was first evaluated before use. In order to observe the effect of the plenum on acoustic wave induced on the burner, the velocity disturbances at the burner entrance is compared to the acoustic intensity produced by the speakers. The plenum gas volume is also numerically analyzed to have a better scientific insight. The setup depicted in Fig. 1 consists of the burner, measurement devices, and sound generation equipment. The diagram of Fig. 2 illustrate the relation between the various devices. The devices and their actual accuracies in current experiments are listed in Table 1.

The burner

The tests are conducted using an atmospheric confined burner operating on air and natural gas in fully premixed mode. The burner is of medium swirl type and utilizes a central bluff-body to enhance stability. A quartz tube of 75 mm inner diameter and 100 mm length circumscribes the flame. This burner was previously used for flame stability limits analysis. Burner details are completely described in reference [45]. Acoustically excited flame dynamics are known to make premixed flames more prone to upstream propagation [46]. In the previous study, several bluff-bodies were examined. Y14 configuration that consisted of a central bluff-body with upper section diameter of 14 mm proved to be the most resistant one against flashback. It was thus chosen for the majority of flame dynamics studies. However, few test were conducted with Y11 configuration. The burner operates at thermal power of 3.2 kW and 35% excess air.

Fig. 1 Experimental setup including the burner, sensors, and the data acquisition box

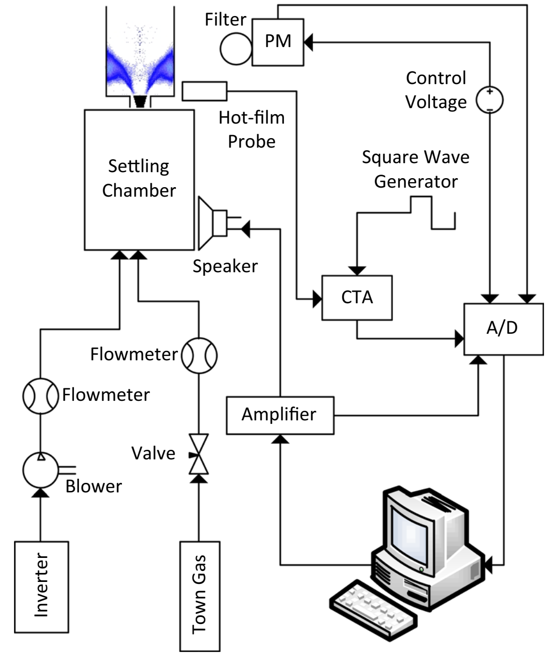

Fig. 2 Schematic of the experimental setup and measurement devices layout

Reynolds number, based on the nozzle diameter and average exit velocity is 3100.

Air and natural gas first enter a settling chamber on which the loud speakers are installed as shown in Fig. 3. Acoustic wave generated by the speakers can possibly affect the instantaneous massflow of air and gas through the feed lines, thereby varying the equivalence ratio entering the chamber. Nevertheless, mixture velocity in the settling chamber is so low that the equivalence ratio wavelength becomes short and these waves essentially vanish while going through the long chamber. This is another benefit of the settling chamber in addition to destroying large-scale turbulent eddies. Finally, a flow straightener is installed above the loud speakers followed by a divergence section leading to the burner.

Measuring instruments

Flame chemiluminescence intensity is measured using a Thorlabs PMM01 photomultiplier, covered with an ASAHI Spectra XBPA310 UV optical filter with center wavelength

Table 1 Measuring devices and their accuracies

Device	Property measured	Accuracy
Hot film anemometer	Velocity	1.5%
Photomultiplier	Chemiluminescence	5%
Air flowmeter	Air volumetric flowrate	0.2 m^3 hr^{-1}
Gas flowmeter	Town gas volumetric flowrate	0.1 Lit hr^{-1}

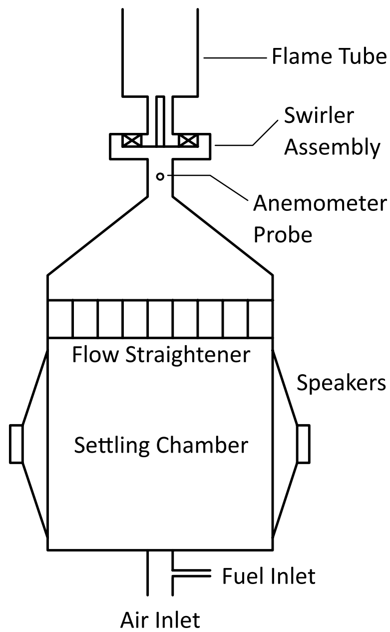

Fig. 3 Schematic of the burner configuration

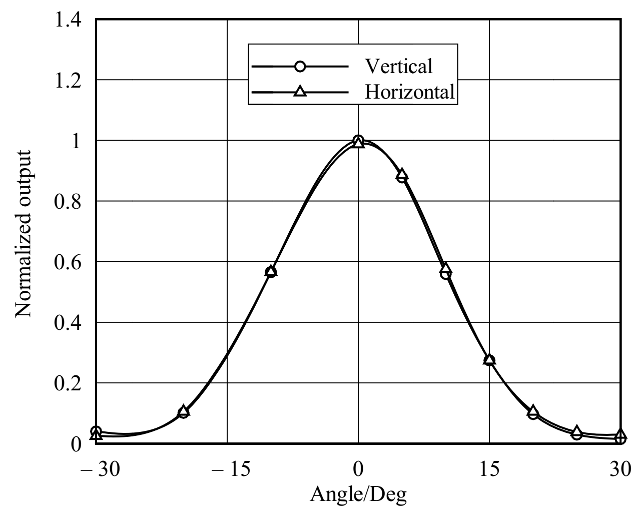

Fig. 4 Photomultiplier angular response to incident light

of 310nm and width of 10nm. This wavelength is related to OH* radicals. Regular environmental lights do not affect the photomultiplier at this wavelength and the laboratory need not be dark. The sensor output is linearly proportional to received radiations and need not be calibrated, since the relative fluctuations of chemiluminescence intensity is to be measured. The device settling time is 15μs which is suitable for capturing fluctuations of up to 20 kHz.

The PM angular response is not mentioned in its specification nor is it usually discussed in studies concerning flame measurement response. It was thus necessary to be examined. An LED was placed at a certain distance from the PM but at various angles with respect to the PM axis in both vertical and horizontal planes. The output voltage is shown in Fig. 4. Sensitivity to received light is strongly dependent on the angle of incidence. The recording is noticeably lower for lights incident from the sides. Fortunately, its behavior is the same for vertical and horizontal planes. According to these findings, the PM was installed far from the flame at a distance of 70 cm. At this distance, the flame is seen within ± 2.8 degrees angle by the sensor. Flame chemiluminescence at its edges is received 5% weaker than its center. This is an inevitable error of the measurements.

Instantaneous velocity of flow just upstream of the swirler assembly was measured with a constant-temperature anemometer utilizing a hot-film probe for which calibration process over the appropriate velocity range is presented in [47]. It was comprised of a TSI 1210-20 cylindrical hot-film probe and TSI 1750 constant temperature controller. In order to examine the frequency response, a step change should be sent to one side of the controller bridge to observe how the anemometer responds. A square wave is a good choice since it can be monitored on an oscilloscope. The probe of the device was installed in the flow and a 1 kHz square wave of 300 mV amplitude generated by the acquisition device was sent to the controller under no-flow condition and also in a flow velocity of 8.7 m s^{-1}. The output is shown in Fig. 5. The frequency response is the reciprocal of the pulse width (70 and 35 micro seconds): 14 and 28kHz for no-flow and 8.7 m s^{-1} flow, respectively. These are far above the frequencies studied.

In order to determine the uncertainty of the photomultiplier and the anemometer, measurements were repeated several times for the same flame and flow conditions. Uncertainty is calculated as the largest relative deviation from the mean value. The result of every measurement along with the corresponding mean value and uncertainty is listed in Table 2. In the case of the flowmeters, this process was not applicable, because they are inline instruments that cannot be taken out and put back in again to repeat a measurement. Instead, uncertainty for such instruments may be determined based on the scale provided on them. The value read on the gas flowmeter is 4.9 lit min^{-1} and there are graduations every 0.5 lit min^{-1} on this instrument. The uncertainty of a reading is thus half the distance between graduations, i.e., 0.25 lit min^{-1} or equivalently 5%. The uncertainty of the air flowmeter becomes 4% through the same method.

The signals from the CTA, PM, and the speakers input voltage are recorded at a rate of 10 thousand samples per second. The sinusoidal signal sent to the two 8 Ohm speakers have a tailored amplitude pattern. For each specific frequency and amplitude to be studied, the amplitude was gradually increased from zero to the desired value within one second, held constant for three seconds, and then the

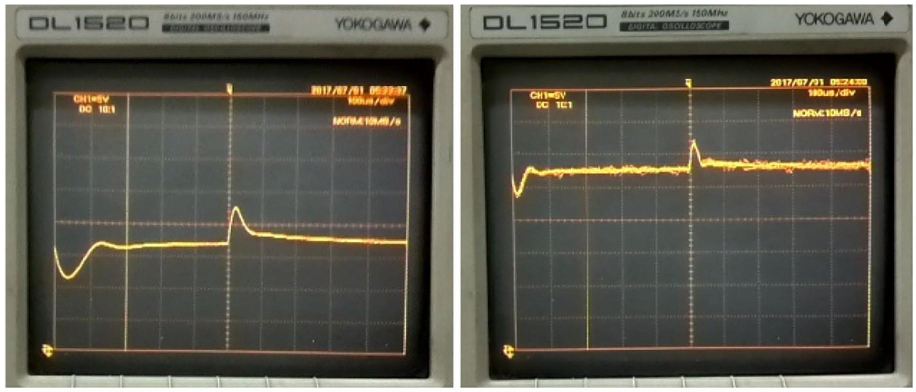

Fig. 5 Anemometer output in square wave test to examine frequency response. Horizontal axis span is 1 milliseconds, vertical axis is output voltage

Table 2 Uncertainty analysis for the PM (Volts unit) and the CTA (m^3 hr^{-1} units)

Equipment	Measurements			Mean	Uncertainty
PM	2.952	2.982	2.977	2.992	1.9%
	3.001	3.048			
CTA	4.374	4.450	4.488	4.443	1.5%
	4.456	4.467	4.412		
	4.455				

excitation was stopped. It was observed that no transient effect is observed through this gradual pattern.

Numerical details

In order to obtain natural frequencies and mode shapes of the gas volume, the homogenous form of Eq. (8) was solved using the commercial software COMSOL 5.2. The upper plane of the settling chamber may be considered a closed boundary since a duct with a large cross-section meets a narrow one and the majority of the traveling waves are reflected as a result. The same rule holds for the bottom of the settling chamber. The ducts downstream of the settling chamber and the swirler assembly have short length scales and thus have high natural frequencies which are too above the frequencies studied. Therefore, these sections did not need to be analyzed. Based on these simplifying assumptions, the acoustic behavior of the settling chamber only needed to be analyzed. The pressure derivative was set to zero on all boundaries because of no-flow condition. Figure 6 shows this domain with a 3340-element mesh. The problem was also solved with a finer mesh arrangement containing 17,800 elements. In both cases, the solution took only few seconds and the results were the same independent of the mesh size. Sound velocity in air is the only constant of the solved equation which is 346 m s^{-1} at 25 °C. It is an eigenvalue problem whose solution gives the natural frequencies and mode shapes.

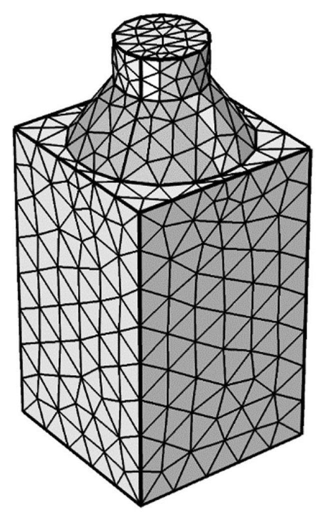

Fig. 6 Domain of the numerical simulation to obtain natural frequencies and mode shapes

Results and discussion

The flame was ignited with the above-mentioned fuel and air flow rates. At this excess air ratio, the dominant radiation from the flame in the visible spectrum is the 430 nm emission of the CH* decaying radicals that gives the flame a violate-blue color. Using chemical equilibrium analysis code CEA, the adiabatic flame temperature was found to

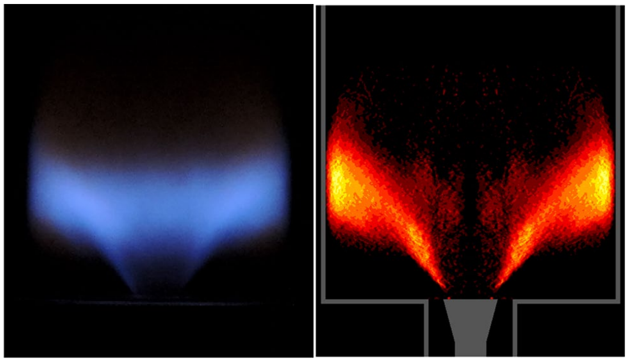

Fig. 7 Normal (top) and chemiluminescense (bottom) after Abel transform images of the steady flame

be 1900 K. Steady state flame is shown in Fig. 7. The processed image is after Abel transform that shows the flame in its axisymmetry plane.

The service temperature of the quartz tube used as combustion chamber is merely 1350 K. The tube is in contact with the room atmosphere and its temperature is certainly lower than the hot product gases. That is why, after hours of operation, no deformation, crack, opaqueness, nor particle deposition was seen on the quartz tube. Therefore, the flame tube needs no cooling which may undesirably affect the flame operation or the process of chemiluminescence detection.

Acoustic excitation with frequencies of 50–500 Hz and various intensities were examined. With Y11 configuration, although a high excess air ratio was selected to be far away from flashback, the flame encountered upstream propagation when excitation intensity is increased. It entered the settling chamber and made the fresh mixture explode. This showed that upstream flow fluctuation can enhance flame flashback. This problem is not observed with Y14 configuration with which all the following results are obtained.

Three signals of speaker input, anemometer output, and photomultiplier output were simultaneously recorded and then analyzed. Frequency and amplitude were obtained through the well-known method of Fourier transform. There is a simple and frequently-used method for calculation of the phase difference between signals. It consists of observing and comparing the instants of time when the signals climb up their mean values. This method was first examined but failed to give repeatable results. Alternatively, phase difference was obtained by a new method. In this method, a function $C(\tau)$ representing coincidence quality of the two signals f(t) and s(t) one of which given a time shift of τ was established:

$$C(\tau) = \int f(t+\tau) \cdot s(t)\mathrm{d}t. \tag{9}$$

The phase difference was related to the time shift value τ that maximizes the coincidence quality function as $\varphi = 2\pi f \tau$. Figure 8 illustrates an example of such a function for coincidence of heat-release on speaker signal for 250 Hz.

Acoustic behavior of the setup

The response of the burner to acoustic excitation by the loud speakers is discussed in this sub-section. As the excitation frequency increases, fluctuating velocity noises weakened, even at high excitation levels. Figure 9 compares acoustic velocity for 50 and 350 Hz for instance. The sampling rate was high enough for possible noises to be discovered. The difference in smoothness is therefore a physical reality. The reason must be the fact that disturbances roused unintentionally have frequencies higher than that of the forced excitation and high-frequency disturbances vanish more easily.

The acoustic behavior of the chamber was not the same for the range of frequencies studied. At some frequencies, a strong unwanted fluctuation with a frequency of about 300 Hz was observed. Furthermore, acoustic excitation at 300 Hz turned out to reach very high levels. Flow fluctuation amplitude is shown in Fig. 10 for a 150 Hz test. The amplitude of the induced 300 Hz fluctuation compares with the forced one. A weak 450 Hz peak is also observed which is the third harmonic. The uprise of second harmonic was seen for other frequencies too, as shown for instance in Fig. 11 for a 250 Hz test, but not with such a high amplitude. This hypothesis soon came to mind that the settling chamber faces a resonance. Natural frequencies and mode shapes of the chamber was studied through solution of the homogenous form of Eq. (8) as explained in Sect. 3.3 to see if this guess was true. The first four mode shapes are depicted in Fig. 12. The first natural frequency was 288 Hz that was very close to the

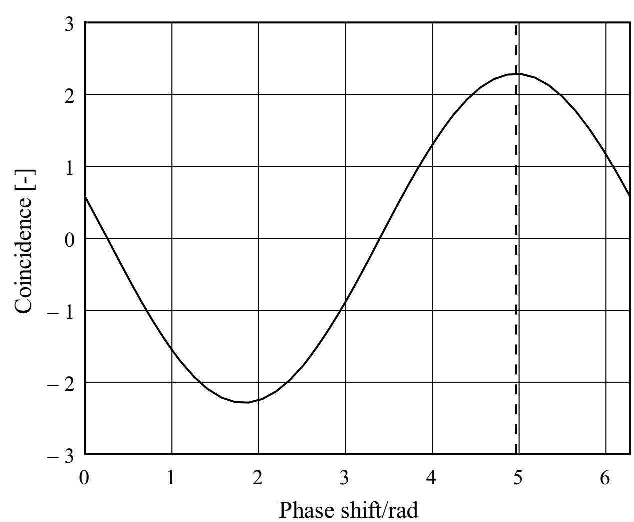

Fig. 8 Coincidence criteria of heat-release on speaker signal over a full period for excitation at 250 Hz

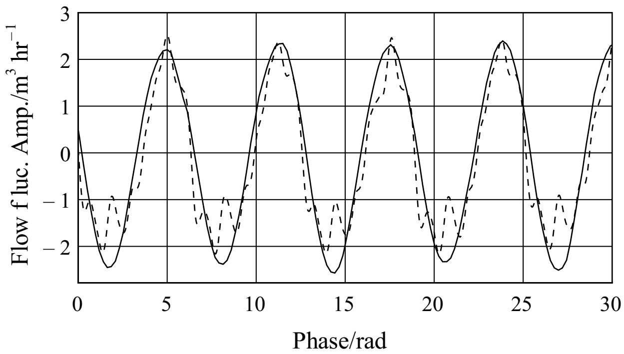

Fig. 9 Flow fluctuation amplitude measured at nozzle entrance for excitations at 50 (—) and 350 (—) Hertz

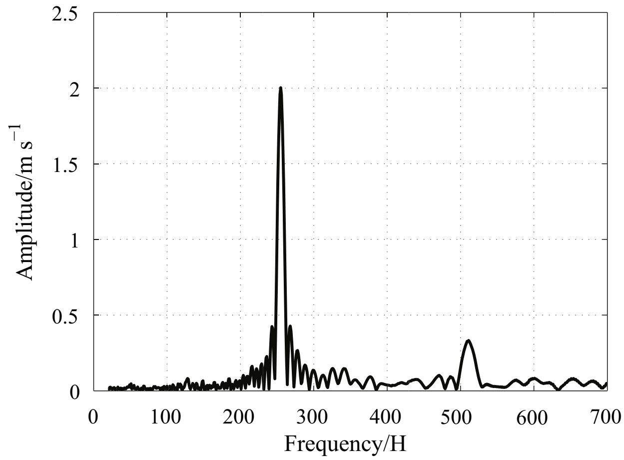

Fig. 11 Flow fluctuation amplitude versus frequency for a 250 Hz test

observed resonant frequency. The assumption that the swirl assembly above the settling chamber and the feed lines may be ignored and omitted from the computation also proved to be valid.

Nonetheless, resonance at or near natural frequencies other than the first one (i.e., 526, 533, and 631 Hz) was never observed. The reason for this must lie in the position of the speakers with respect to the mode shapes. The speakers located at lower half of two opposing sides of the chamber. The first mode had pressure antinodes at these locations. On the contrary, the second mode had nodes at both of the speakers. In the case of the third and fourth mode shapes, the mode shape state at speaker locations were in opposite phase so that they interfere destructively. Thus, the first mode only could be excited.

This chamber resonance had consequences. If the chamber was designed with an adjustable length, the natural frequency could be set on the value under study in order to reach very high excitation levels with small acoustic power. Additionally, unwanted acoustic excitation might be avoided. 100 and 150 Hz frequencies were not included in this study just because of this (in some cases unwanted) effect. Second harmonics at very low levels were observed in 125 and 250 Hz cases but it must not interfere with obtaining flame response especially because amplitude of each fluctuation was calculated separately.

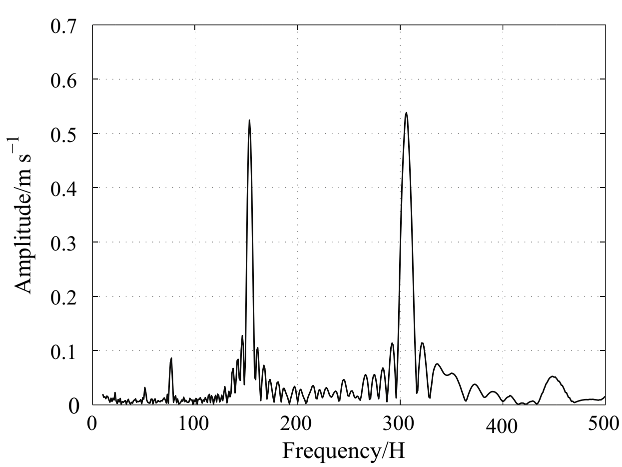

Fig. 10 Flow fluctuation amplitude versus frequency for a 150 Hz test

Mass flow fluctuation level varied linearly with speaker voltage for a specific frequency as shown in Fig. 13. Proportionality coefficient is shown in Fig. 14. This was not due to nonlinearity of the speakers because acoustic gain of a speakers is the same over its operating frequency range. This was a characteristic of the settling chamber geometry. For a first-order system, response function to forced vibration obeys the following relation:

$$RF = \frac{1}{\sqrt{\left(1 - \left(\omega/\omega_{\mathrm{n}}\right)^2\right)^2 + \left(2\zeta\omega/\omega_{\mathrm{n}}\right)^2}} \quad (10)$$

where ω and ω_{n} are forced and undamped frequencies, respectively, and ζ is damping coefficient. This function with unknown ω_{n} and ζ was fitted to data of Fig. 14. It is observed that the acoustic behavior of the chamber resembles a first-order system with the peak occurring at the natural frequency.

Flame response

In this sub-section, the dynamics of the flame under acoustic excitation is discussed. With the ultra-violet filter in front of the photomultiplier, environmental light could not affect the detection technique as the PM output was zero in the absence of the flame. Nevertheless, the laboratory was darkened during the chemiluminescence measurement for confidence.

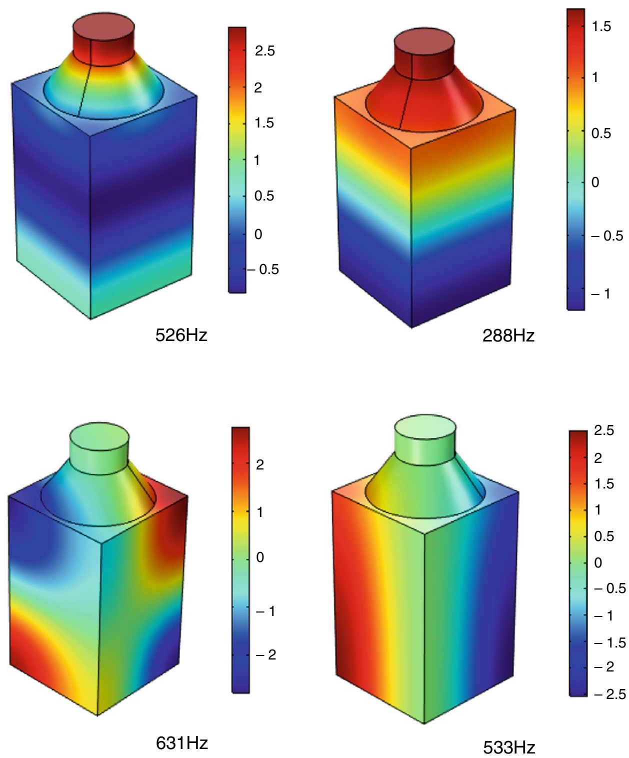

Fig. 12 Natural frequency and mode shapes of the gas volume pressure, units arbitrary

Among the numerous tests, heat-release fluctuation due to acoustic excitation for 125 and 350 Hz are shown in Figs. 15 and 16, respectively, for instance. In 125 Hz case, the time series may appear to include a single sine but FFT (plotted in Fig. 17), revealed a 250 Hz fluctuation too. In fact, the second acoustic harmonic was stimulated inside the settling chamber and manifested itself in the flame heat-release response. Such induced fluctuations were not observed in the case of other frequencies. For example, FFT result in 350 Hz case is shown in Fig. 18 where a broad range of frequencies were sought for possible second or third harmonics.

In the following Figs. 19–23, both heat-release and flow fluctuation levels are plotted versus speaker power. During combustion instability occurrence, frequency remains approximately constant but fluctuations amplitude grows from small values to the limit cycle level. Thus, the flame response behavior as a function of excitation level is worth study. If the response magnitude continued to grow linearly with excitation, instability level would unlimitedly grow too. As Figs. 19–22 show, despite flow, heat-release amplitude did not change linearly over the entire excitation level. It ceased to follow its initial linear growth after a certain excitation level. The threshold amplitude depended on frequency and seems to increase with frequency. In 400 Hz case, the expected nonlinearity is not observed in Fig. 23 probably because the threshold excitation level could not be reached with the setup.

The flame heat-release-rate oscillates at the frequency of the velocity excitation. Fluctuations amplitude is a function of both frequency and excitation level as shown in Fig. 24. As an example, when the velocity excitation is 60% at 250 Hz frequency, heat-release-rate fluctuates with an amplitude of 55%, i.e., between 1.6 and 4.8 kW. On the other hand, heat-release-rate fluctuation may be nearly zero in response to excitation under some conditions like what happened at 400 Hz. The results are hereafter presented and discussed in relative form instead of absolute form as Eqs. 4 and 8 suggest. The equivalence ratio of the mixture delivered to the flame remained constant during the excitation. This was the flame shape and its area that changed cyclically and the rate of the fresh mixture consumption fluctuated as a result.

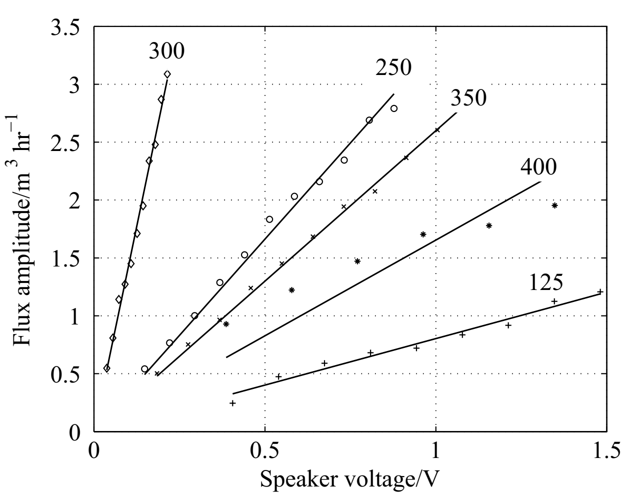

Fig. 13 Nozzle flow fluctuation relation with speaker input power

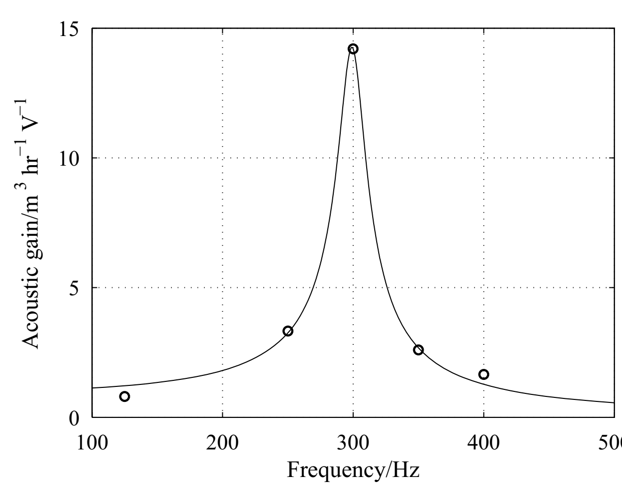

Fig. 14 Ratio of flow fluctuation level to speaker power input over the frequency range; experimental data (circles) and fitted first-order system response function (line)

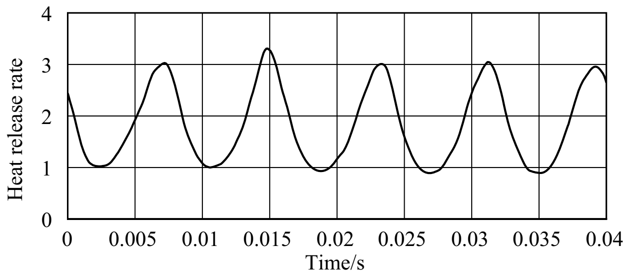

Fig. 15 Heat-release fluctuation under 125 Hz excitation

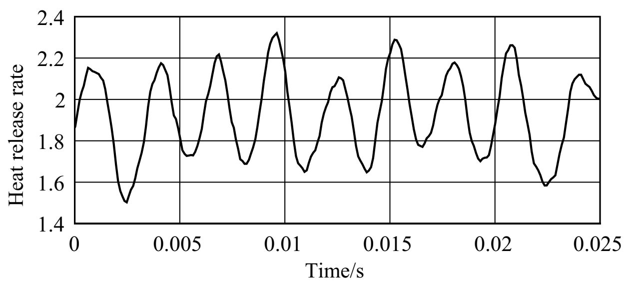

Fig. 16 Heat-release fluctuation under 350 Hz excitation

Dividing the amplitudes of heat-release and velocity by their respective mean values gives the transfer function as introduced by Eq. 4. The acoustic field behavior remains linear from instability onset to its limit cycle and this is the flame response that causes the nonlinear behavior. Therefore, the way that the response of a flame changes with respect to excitation amplitude growth is of importance for evaluation of instability level. Transfer function magnitude is plotted in Fig. 25 for 125 and 250 Hz cases and in Fig. 26 for 300, 350, and 400 Hz cases. They are shown in separate figures because the function magnitude for lower frequencies were pretty higher than those for higher frequencies. Excitation at 500 Hz and higher frequencies was also applied to the burner but almost no response could be seen in the heat-release. Response nonlinearity is clear again since the magnitude varies with the excitation level. For 300 and 350 Hz cases, the flame shows linear behavior under excitation levels lower than 50% and experience nonlinearity for higher levels.

The describing function phase is shown in Fig. 27. The closer the frequency is to the natural frequency, the broader range the corresponding curve covers. The describing function phase, unlike the magnitude, does not vary with excitation level but is strongly dependent on frequency. The higher the frequency, the bigger the describing function phase. Remember that this phase difference φ was calculated based on the time difference τ between velocity and heat-release (i.e., $\varphi = 2\pi f \tau$). The observed approximate proportionality of phase to frequency, implies that the time difference between velocity and heat-release fluctuations are nearly the

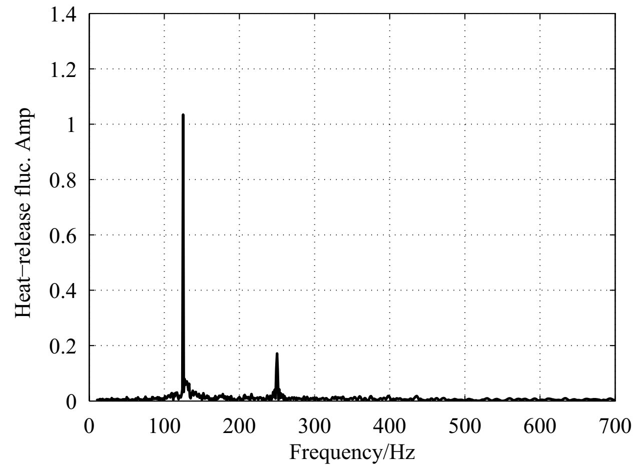

Fig. 17 Frequency of harmonic fluctuations found under 125 Hz excitation

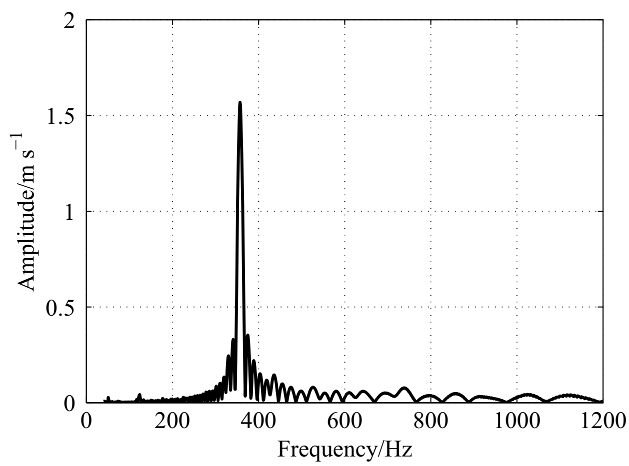

Fig. 18 Frequency of harmonic fluctuations found under 350 Hz excitation

same for all conditions. The phase difference is produced by the time delay it takes for the waves to travel from the velocity measurement point to the flame. This hypothesis is essential to develop a model for flame response based on distributed time delays [48].

The validity of assigning a global describing function to the flame may now be discussed. In order to perform this validation one need to compare the flame dimension with the wavelength. The smallest wave length corresponds to the highest frequency and the lowest sound speed. In a real combustor, the temperature varies with position due to addition of cooling air and so does the sound speed. The wave form is thus different from a simple sinusoidal shape. However, the wave form at flame volume must be taken into account and its complexity is of no importance. The flame temperature of

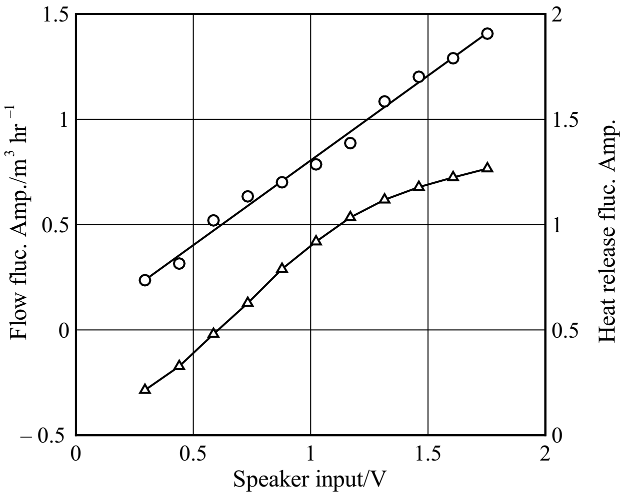

Fig. 19 Flow (circles) and heat-release (delta) fluctuation level versus speaker power in 125 Hz case

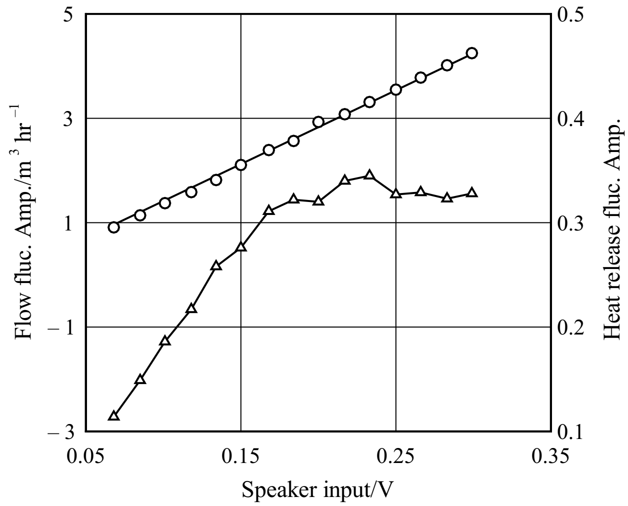

Fig. 21 Flow (circles) and heat-release (delta) fluctuation level versus speaker power in 300 Hz case

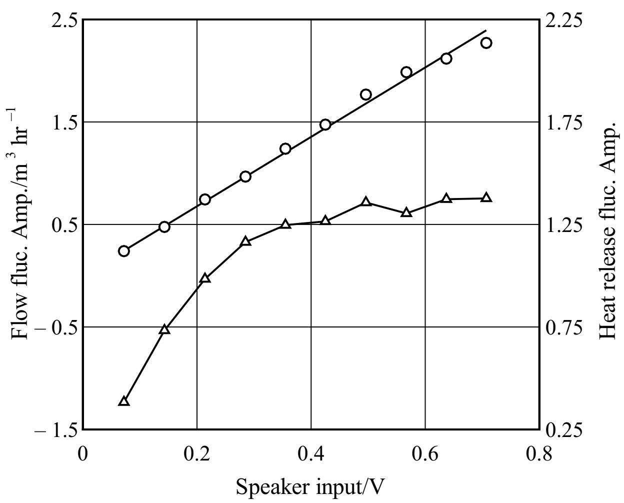

Fig. 20 Flow (circles) and heat-release (delta) fluctuation level versus speaker power in 250 Hz case

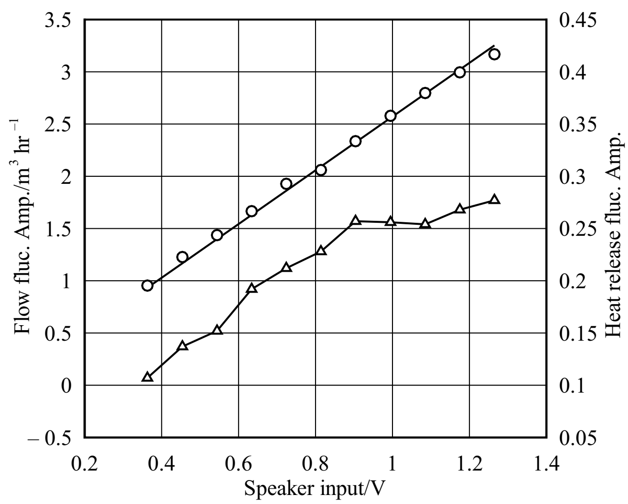

Fig. 22 Flow (circles) and heat-release (delta) fluctuation level versus speaker power in 350 Hz case

current experiments was obtained to be 1900K which results in 815 ms^{-1} sonic velocity. The highest frequency on the other hand, at which a response may be sensed, is 400 Hz. The wavelength under these conditions is 2.1 m, 30 times the flame length, that is only 0.07 m. This means that the flame occupies π/15 phase of the wave and the whole flame can be well considered to be at the same phase or in other words it is regarded as compact. For lower frequencies, the wave is longer and the flame is considered more compact. For higher frequencies, the response is too weak to trigger an instability. Therefore, as far as the interaction of heat-release with the acoustic field is to be considered, assigning a global response or using a field function would give the same results.

Concluding remarks

Response of a premixed natural gas flame with thermal power of 3.2 kW and 35% excess air to acoustic excitation was studied. This laboratory burner was stabilized via a radial swirler and a conical bluff-body, equipped with a settling chamber. Not only the response but also the

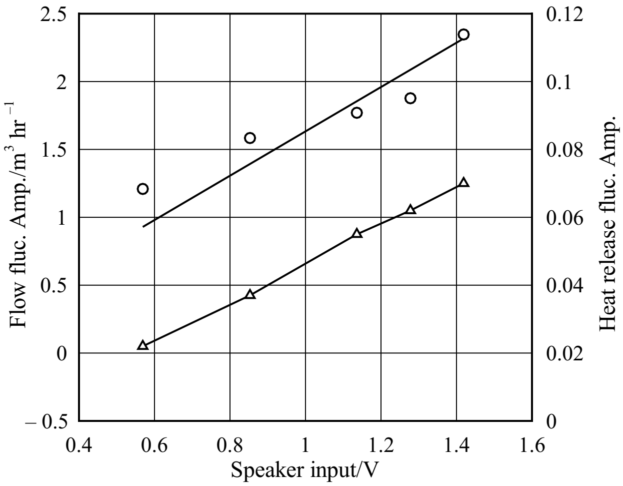

Fig. 23 Flow (circles) and heat-release (delta) fluctuation level versus speaker power in 400 Hz case

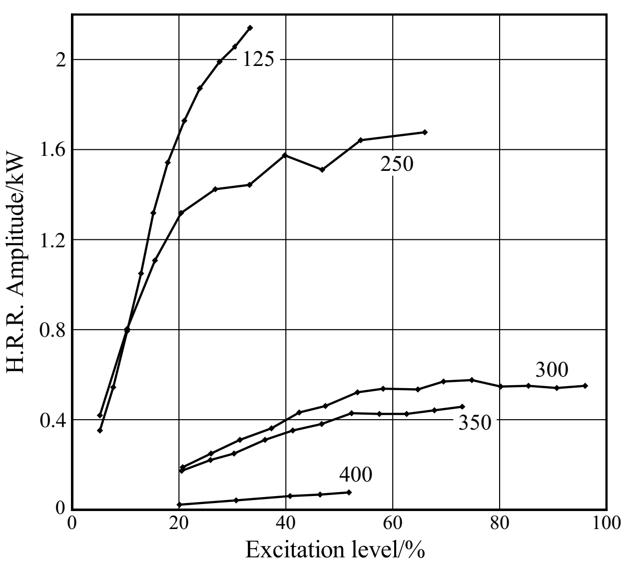

Fig. 24 Heat-release-rate (H.R.R) fluctuation amplitude as a function of excitation level for various frequencies (curve labels)

experimental issues engaged in obtaining the response is surveyed. The conclusions are:

1 Photomultiplier gain in vertical and horizontal planes were the same but strongly dependent on angle of incident. The device sensitivity was the highest for the front and falls at the sides. The flame should therefore be in a small view angle in front of the device for better accuracy.
2 Inlet velocity fluctuations could render a normally stable flame unstable and cause explosive flashback. This upstream propagation happened for the smaller bluff-body which had a narrower stable operating map.

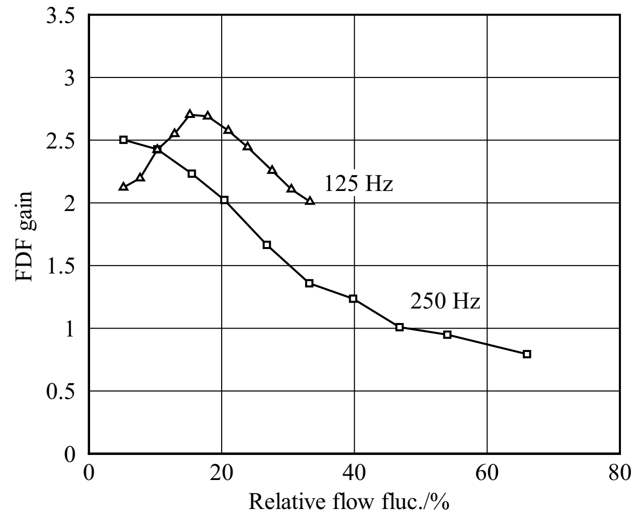

Fig. 25 Transfer function magnitude for 125 and 250 Hz excitation

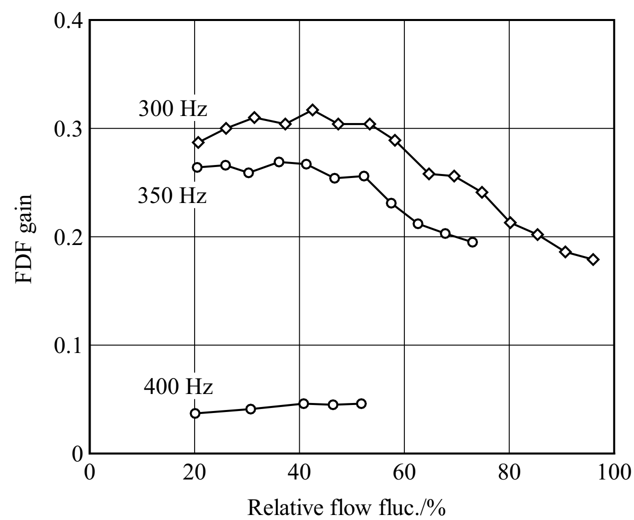

Fig. 26 Transfer function magnitude for 300, 350, and 400 Hz excitation

3 Among natural mode shapes, the one for which in-phase antinodes lie on loudspeakers was augmented. High excitation level with low input energy was achieved at corresponding natural frequency. However, frequencies that are devisors of this natural frequency may not be studied easily.
4 Flame describing function might be constant for lower excitation levels but it followed a falling trend for higher levels. Having a reverse dependency on frequency, FDF reached values as high as 2.5 for low and as low as 0.05 for high frequencies. No sensible respond to 500 Hz or higher frequencies could be observed.
5 FDF phase showed negligible dependency on excitation level but was approximately proportional to frequency.

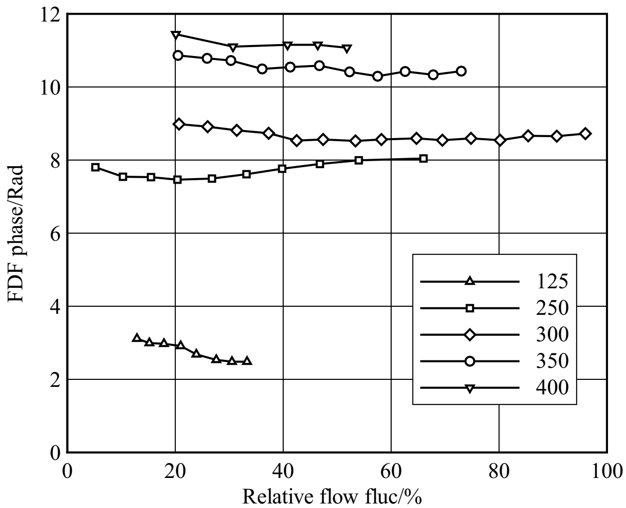

Fig. 27 Describing function phase for various frequencies

This implied that the time delay due to wave travel determined the phase.

6 The fact that the whole flame occupied a small part of the acoustic wave length renders assuming a global FDF justifiable.

For future activity it is suggested that (a) the effect of bluff-body configuration on acoustic response and (b) effect of acoustic excitation on flashback limits for various bluff-bodies, be studied.

Authors contributions All authors contributed to the study conception and design. Conceptualization, investigation, formal analysis, methodology, and writing were performed by MB. EM supervised the research. Project administration were done by FO. All authors read and approved the final manuscript.

Declarations

Conflict of interest The authors have no relevant financial or non-financial interests to disclose.

References

1. Lefebvre AH, Ballal DR. Gas turbine combustion. CRC Press; 2010. https://doi.org/10.1201/9781420086058.
2. Dunn-Rankin D. Lean combustion: technology and control. Academic Press; 2008.
3. Lieuwen T, Yang V. Combustion instabilities in gas turbine engines: operational experience, fundamental mechanisms and modeling. American Institute of Aeronautics and Astronautics; 2005.
4. Avdonin A, Meindl M, Polifke W. Thermoacoustic analysis of a laminar premixed flame using a linearized reactive flow solver. Proc Combust Inst. 2019;37(4):5307–14.
5. Guo S, Silva CF, Ghani A, Polifke W. Quantification and propagation of uncertainties in identification of flame impulse response for thermoacoustic stability analysis. J Eng Gas Turbines Power. 2019;141(2):021032–110.
6. Li Q, Dong F, Liu P. A numerical study on the acoustic forcing of a laminar premixed saturated spray flame. J Therm Anal Calorim. 2020;139:2899–912.
7. Dowling AP, Stow SR. Acoustic analysis of gas turbine combustors. J Propul Power. 2003;19(5):751–65.
8. Huang Y, Yang V. Dynamics and stability of lean-premixed swirl-stabilized combustion. Prog Energy Combust Sci. 2009;35:293–364.
9. Poinsot T. Veynante D. Theoretical and numerical combustion. Edwards; 2001.
10. Silva CF, Nicoud F, Schuller T, Durox D, Candel S. Combining a helmholtz solver with the flame describing function to assess combustion instability in a premixed swirled combustor. Combust Flame. 2013;160:1743–54.
11. Palies P, Durox D, Schuller T, Candel S. Nonlinear combustion instability analysis based on the flame describing function applied to turbulent premixed swirling flames. Combust Flame. 2011;158:1980–91.
12. Han X, Morgans AS. Simulation of the flame describing function of a turbulent premixed flame using an open-source LES solver. Combust Flame. 2015;162:1778–92.
13. Behzadi M, Farshchi M. Numerical investigation of laminar premixed conical flame response to acoustic excitation. J Space Sci Technol. 2015;8(1):9–18 (**in Persian**).
14. O'Connor J, Acharya V, Lieuwen T. Transverse combustion instabilities: acoustic, fluid mechanic, and flame processes. Prog Energy Combust Sci. 2015;49:1–39.
15. Smith T, Emerson B, Proscia W, Lieuwen T. Role of induced axial acoustics in transverse acoustic flame response. Combust Flame. 2018;195:140–50.
16. Oberleithner K, Schimek S, Paschereit CO. Shear flow instabilities in swirl-stabilized combustors and their impact on the amplitude dependent flame response: a linear stability analysis. Combust Flame. 2015;162:86–99.
17. Kim D, Park SW. Forced and self-excited oscillations in a natural gas fired lean premixed combustor. Fuel Process Technol. 2010;91:1670–7.
18. Paschereit CO, Schuermans B, Polifke W, Mattson O. Measurement of transfer matrices and source terms of premixed flames. J Eng Gas Turbines Power. 2002;124:239–47.
19. Cosic B, Terhaar S, Moeck JP, Paschereit CO. Response of a swirl-stabilized flame to simultaneous perturbations in equivalence ratio and velocity at high oscillation amplitudes. Combust Flame. 2015;162:1046–62.
20. Ghani A, Albayrak A. From pressure time series data to flame transfer functions: a framework for perfectly premixed swirling flames. J Eng Gas Turbines Power. 2023;145(1):011005–9.
21. Docquier N, Candel S. Combustion control and sensors: a review. Prog Energy Combust Sci. 2002;28:107–50.
22. Shen W, Xing C, Liu L, Hu Q, Wu G, Yang Y, Wu S, Qiu P, Wu J. Chemiluminescence-based characterization of heat release rate dynamic in a micro gas turbine combustion chamber. J Energy Inst. 2022;102:32–41.
23. Karimi N, Brear MJ, Jin SH, Monty P. Linear and non-linear forced response of a conical, ducted, laminar premixed flame. Combust Flame. 2009;156:2201–12.
24. Malaczynski G, Roth G, Johnson D. Ion-sense-based real-time combustion sensing for closed loop engline control. SAE Int J Engines. 2013;6:267–77.
25. Mehta GK, Ramachandra MK, Strahle WC. Correlations between Light Emission, acoustic emission and ion density in

premixed turbulent flames. Symp Combust. 1981;18(1):1051–9. https://doi.org/10.1016/S0082-0784(81)80109-9.

26. Higgins B, McQuay MQ, Lacas F, Rolon JC, Darabiha N, Candel S. Systematic measurements of OH chemiluminescence for fuel-lean, high-pressure, premixed, laminar flames. Fuel. 2001;80:67–74.
27. Higgins B, McQuay MQ, Lacas F, Candel S. An experimental study on the effect of pressure and strain rate on CH chemiluminescence of premixed fuel-lean methane/air flames. Fuel. 2001;80:1583–91.
28. Arghode VK, Khalil AEE, Gupta AK. Fuel dilution and liquid fuel operational effects on ultra-high thermal intensity distributed combustor. Appl Energy. 2012;95:132–8.
29. Moeck JP, Oevermann M, Klein R, Paschereit CO, Schmidt H. A two-way coupling for modeling thermoacoustic instabilities in a flat flame Rijke tube. Proc Combust Inst. 2009;32:1199–207.
30. Swain W, Yejun W, Parajuli P, Hay M, Saylam A, Dreier T, Schulz C, Kulatilaka W. Characterization of a high-pressure flame facility using high-speed chemiluminescence and OH LIF imaging. Exp Fluids. 2023;64:71.
31. Kim KT, Lee JG, Quay BD, Santavicca DA. Response of partially premixed flames to acoustic velocity and equivalence ratio perturbations. Combust Flame. 2010;157:1731–44.
32. Sjoholm J, Rosell J, Li B, Richter M, Li Z, Bai XS, Alden M. Simultaneous visualization of OH, CH, CH_2O and toluene PLIF in a methane jet flame with varying degrees of turbulence. Proc Combust Inst. 2013;34:1475–82.
33. Xavier P, Vandel A, Godard G, Renou B, Grisch F, Cabot G, Boukhalfa MA, Cazalens M. Analysis of the flame structure in a trapped vortex combustor using low and high-speed OH-PLIF. ASME Turbo Expo. 2014;4:25207–10.
34. Dhanuka S, Temme JE, Driscoll JF. Unsteady aspects of lean premixed prevaporized gas turbine combustors: Flame–flame Interactions. J Propul Power. 2011;27(3):631–41.
35. Seybert AF. Two-sensor methods for the measurement of sound intensity and acoustic properties in ducts. J Acoustical Soc Am. 1988;83(6):2233–9.
36. Balachandran R, Ayoola BO, Kaminski CF, Dowling AP, Mastorakos E. Experimental investigation of the nonlinear response of turbulent premixed flames to imposed inlet velocity oscillations. Combust Flame. 2005;143:37–55.
37. Birbaud AL, Durox D, Candel S. Upstream flow dynamics of a laminar premixed conical flame submitted to acoustic modulations. Combusion and Flame. 2006;146:541–52.
38. Rao Z, Li R, Zhao P, Wang B, Zhao D, Xie Q. Similarity phenomena of lean swirling flames at different bulk velocities with acoustic disturbances. Chin J Aeronaut. 2023;36(5):18–32.
39. Palies P, Schuller T, Durox D, Candel S. Modeling of premixed swirling flames transfer functions. Proc Combust Inst. 2011;33:2967–74.
40. Han Z, Hochgreb S. The response of stratified swirling flames to acoustic forcing: experiments and comparison to model. Proc Combust Inst. 2015;35:3309–15.
41. Liu W, Xue R, Zhang L, Yang Q, Wang H. Dynamic response of a forced low-swirl premixed flame with acoustic excitation. Flow Turbulence Combust. 2021;108:1139–57.
42. Æsøy E, Nygård T, Worth NA, Dawson JR. Tailoring the gain and phase of the flame transfer function through targeted convective-acoustic interference. Combust Flame. 2022;236:111813–4.
43. Gatti M, Gaudron R, Mirat C, Zimmer L, Schuller T. Impact of swirl and bluff-body on the transfer function of premixed flames. Proc Combust Inst. 2019;37(4):5197–204.
44. Yang Y, Wang G, Wu H, Zhu Z, Ma C, Li J. Investigation of flame and flow response in the swirler with different divergence cups and central body under external excitation. Phys Fluids. 2023;35:064102.
45. Behzadi M, Siyadat SH, Ommi F, Saboohi Z. Study of the effect of bluff body size on stability limits of a premixed natural gas swirl burner. J Therm Anal Calorim. 2022;147:1583–96.
46. Shahsavari M, Farshchi M, Chakravarthy SR, Chakraborty A, Aravind IB, Wang B. Low swirl premixed methane-air flame dynamics under acoustic excitations. Phys Fluids. 2019;31:095106.
47. Behzadi M, Ahmadi MH, Ommi F. Hot-wire/hot-film calibration for low velocities using image processing. Sci Iran B. 2021;28(1):265–72.
48. Polifke W. Modeling and analysis of premixed flame dynamics by means of distributed time delays. Prog Energ Combust Sci. 2020;79:100845.